Journal of *Marine Science and Engineering*

MDPI

Article

Fast and Deterministic Underwater Point Cloud Registration for Multibeam Echo Sounder Data

Liang Zhao [1], Lan Cheng [1], Tingfeng Tan [2], Chun Cao [2] and Feihu Zhang [2,*]

[1] College of Electrical and Power Engineering, Taiyuan University of Technology, Taiyuan 030024, China; zhaoliang163yz@163.com (L.Z.); taolan_1983@126.com (L.C.)
[2] School of Marine Science and Technology, Northwestern Polytechnical University, Xi'an 710072, China; ttf@mail.nwpu.edu.cn (T.T.); caochun@mail.nwpu.edu.cn (C.C.)
* Correspondence: feihu.zhang@nwpu.edu.cn

Abstract: Investigating underwater environments using Multi-Beam Echo Sounder (MBES) point cloud registration technology is a critical yet underdeveloped area in oceanographic research. This paper presents a fast, deterministic Branch-and-Bound (BnB) method with four degrees of freedom, which combines Inertial Measurement Unit (IMU) data with MBES point cloud data for precise registration. Given the prevalence of outliers and noise in underwater acoustic measurements, the BnB method is employed to provide globally deterministic solutions. However, due to the exponential convergence speed of the BnB method with respect to the dimensionality of the solution space, searching within a six-degree-of-freedom parameter space (three rotational and three translational degrees of freedom) can be extremely time-consuming. To this end, the Z-axis of the point cloud is aligned with the gravitational direction of the IMU, reducing the rotational degrees of freedom from three to one, specifically concerning yaw. Additionally, an outlier exclusion strategy is introduced to eliminate mismatches, significantly reducing the number of key-point correspondences and thereby improving registration efficiency. Experiments conducted on both public and real-world lake datasets demonstrate that the proposed method achieves a favorable balance between speed and accuracy, outperforming other tested methods and meeting the demands of contemporary research.

Keywords: underwater point cloud registration; correspondence-based registration; multibeam echo sounder (MBES); branch and bound (BnB)

check for updates

Academic Editors: João Miguel Dias and Salman Nazir

Received: 27 August 2024
Revised: 13 December 2024
Accepted: 26 December 2024
Published: 28 December 2024

Citation: Zhao, L.; Cheng, L.; Tan, T.; Cao, C.; Zhang, F. Fast and Deterministic Underwater Point Cloud Registration for Multibeam Echo Sounder Data. *J. Mar. Sci. Eng.* **2025**, *13*, 26. https://doi.org/10.3390/jmse13010026

Copyright: © 2024 by the authors. Licensee MDPI, Basel, Switzerland. This article is an open access article distributed under the terms and conditions of the Creative Commons Attribution (CC BY) license (https://creativecommons.org/licenses/by/4.0/).

1. Introduction

Underwater point cloud registration technology is crucial for applications in marine archaeology, marine biology research, and offshore engineering. It significantly enhances our understanding of the underwater environment and cultural heritage, while also improving the safety and efficiency of marine operations. In marine archaeology, this technology aids in the precise reconstruction of three-dimensional models of sunken ships and ancient ruins. In marine biology, it provides high-accuracy data for monitoring coral reefs and underwater ecosystems. For offshore engineering, underwater point cloud registration ensures the accuracy of seabed surveys, thereby enhancing the safety of engineering design and construction [1–4]. The Multi-Beam Echo Sounder (MBES), an important sensor in the field of underwater detection, is capable of capturing data over extensive seafloor areas, resulting in dense point cloud datasets. These point cloud datasets are crucial for detailed underwater mapping and in-depth analyses. Currently, research on underwater point cloud registration using an MBES remains relatively scarce. The precision of point clouds

generated by MBESs is susceptible to changes in water properties, such as temperature and salinity. Furthermore, the resolution of these point clouds is significantly lower compared to those obtained from LiDAR, coupled with a substantial amount of noise and number of outliers, which makes underwater point cloud registration particularly challenging.

In [4], a multibeam data processing system was proposed, which integrated sonar parameter configuration, data storage, and point cloud conversion. The iEKF (iterative extended Kalman filter) method was then used to estimate the odometer, and a preliminary point cloud map was constructed. The focus of the work in [4] was on the generation of multibeam point cloud data. Although a simple MBES point cloud registration was attempted using the GICP (Generalized Iterative Closest Point) method in [4], that method is computationally intensive, slow, and sensitive to noise. This paper further investigates the MBES point cloud registration method proposed in [4]. Additionally, the point cloud data used in the experiments of this study were all generated by [4].

Existing point cloud registration technologies can generally be divided into two types [5]: correspondence-based and correspondence-free methods. Correspondence-free methods [6] rely on the global features or statistical information of point clouds. Although these methods are faster, their robustness is somewhat limited. In contrast, correspondence-based methods [7–10] rely on explicit local features to achieve precise point cloud registration, typically providing higher accuracy, but they come with relatively higher computational complexity. Given the requirements for adapting to complex seabed topography, this study primarily adopts the correspondence-based registration approach as its research focus. However, due to the instability of key feature point matching methods [11], mismatches are almost inevitable [7–9]. In this regard, consensus maximization methods [12,13] are widely applied due to their robustness against outliers and noise. Random Sample Consensus (RANSAC) [14] is the most commonly used consensus maximization technique, but it only generates the optimal solution with a certain probability. Recently, BnB methods [15,16] have been used to solve point cloud registration problems based on correspondences, due to their ability to provide definite and effective solutions. Nevertheless, the convergence rate of this method is exponential in relation to the dimensionality of the solution space.

This study focuses on the four-degree-of-freedom problem in the field of underwater point cloud registration. Specifically, given two underwater point clouds, their Z-axes are aligned with the direction of gravity provided by an IMU, resulting in the relative rotation between the point clouds being a pure yaw rotation. Therefore, only one degree of rotational freedom and three degrees of translational freedom need to be estimated between them. The main contributions of this study can be summarized as follows:

1. We propose an efficient and deterministic four-degree-of-freedom underwater point cloud registration method based on the BnB approach, which significantly improves the accuracy and speed of registration. To the best of our knowledge, this is the first application of the BnB method in the field of MBES point cloud registration.
2. Through experimental tests conducted on public datasets as well as underwater scenarios in lake environments, our method shows faster processing speeds and higher accuracy compared to other existing point cloud registration techniques, achieving a favorable balance between efficiency and robustness.

2. Related Work

Currently, although underwater point cloud registration represents a unique and challenging field, existing research methods primarily rely on traditional point cloud registration techniques developed for above-water environments. At present, no dedicated methods are specifically designed for underwater conditions. This section introduces widely used methods within the current point cloud registration domain. Although these methods are not explicitly tailored for underwater environments, they provide a foundational basis and serve as references for the study of underwater point cloud registration.

In the realm of correspondence-free methods, point clouds are aligned directly without the necessity of estimating explicit point correspondences. The Iterative Closest Point (ICP) method [6] is the most prevalent in this category, achieving registration by iteratively selecting point pairs from two point sets to minimize distance. However, this approach is vulnerable to local optima and initial positioning issues [17,18].

In contrast, correspondence-based registration involves two key steps [19]: (1) the extraction of three-dimensional key points [20–23] and the establishment of presumed correspondences using 3D feature descriptors [24], and (2) the estimation of transformation based on the given correspondences. When the correspondences are accurate, a precise solution to the registration problem is attainable. Nevertheless, presumed correspondence outliers are an inevitable aspect of practical applications, necessitating robust registration techniques [8,9]. Consensus maximization, particularly the heuristic RANSAC method [14], is one of the most popular paradigms for addressing robust registration issues. RANSAC uses a minimal solver to calculate rotation and translation separately in each iteration. However, its effectiveness diminishes as the outlier rate increases. Recent variants of RANSAC, such as Graph-cut RANSAC (GCRANSAC) [25], which integrates graph-cut methods to enhance localized optimization, have been proposed to improve performance. Nonetheless, methods based on RANSAC are inherently probabilistic due to the randomness in sampling, yielding correct solutions with certain probabilities [26–28]. In recent years, learning-based methods have shown promising results in the field of point cloud registration. Fully Convolutional Geometric Features (FCGFs) [29] are the first method to densely extract point cloud features using a fully convolutional network based on sparse convolutions. Predator [30] focuses on detecting matching key points in overlapping areas, allowing for the successful registration of point cloud pairs with low overlap rates. However, the high costs associated with collecting underwater MBES data result in a scarcity of open-source datasets. This situation constrains the training effectiveness of neural networks in MBES data processing, making it challenging to achieve ideal performance levels.

To counter these limitations, the Branch-and-Bound (BnB) method [15] is viewed as a promising alternative in point cloud registration due to its ability to provide deterministic solutions. The BnB algorithm is a global optimization method that systematically narrows the search space from the entire solution range into smaller subspaces, bounding each with the optimal solution it could potentially contain. It prunes areas least likely to have the optimal solution, only ceasing once the entire space has been thoroughly explored. Given enough time, it guarantees a globally optimal solution. Considering its principles, BnB offers robust performance in point cloud registration, especially in challenging scenarios with significant noise, occlusions, and outliers. Traditional methods often struggle under these conditions due to sensitivities to initial conditions, but BnB's deterministic nature allows it to handle these challenges adeptly.

However, the application of BnB in point cloud registration is not without its challenges. The most significant challenge is the inherent computational complexity of the method. BnB demands substantial computational resources, which escalate rapidly with increasing data dimensions. This makes real-time applications difficult. To address these

issues, adaptive strategies have been proposed, such as combining BnB with the Fast Marching Method (FMP) algorithm [31]. This hybrid approach accelerates the BnB method, enhancing the efficiency of the registration process. This study extends the LiDAR point cloud registration method presented in [31] to the field of multibeam sonar point cloud registration. The algorithm formulation section of this paper builds upon the theoretical aspects presented in [31].

3. Problem Formulation

By aligning the Z-axis of the coordinate system with the gravity direction provided by the IMU, the relative rotation is reduced to a pure yaw rotation, thereby simplifying the 6-DOF registration problem to a 4-DOF one. This representation is particularly appropriate when utilizing sonar devices.

Let us postulate the point sets designated as $\mathbf{P}$ for the source and $\mathbf{Q}$ for the target, respectively. Within the framework of correspondence-based registration, a collection of putative correspondences $\mathcal{C} = (\mathbf{p}_i, \mathbf{q}_i)_{i=1}^{M}$ is curated through the meticulous matching of elements from the sets $\mathbf{P}$ and $\mathbf{Q}$, where each pair $\mathbf{p}_i$, $\mathbf{q}_i$ embodies coordinates within the three-dimensional Euclidean space, denoted by $\mathbb{R}^3$. Through $\mathcal{C}$, the objective is to deduce the parameters of a 4-DOF rigid transformation that aligns these point sets:

$$\mathbf{R}(\theta)\mathbf{p}_i + \mathbf{t} = \mathbf{q}_i \tag{1}$$

where rotation angle $\theta \in [0, 2\pi]$ and translation vector $\mathbf{t} \in \mathbb{R}^3$.

Since $\mathcal{C}$ contains outliers, we seek the parameters $\theta, \mathbf{t}$ that maximize the objective function

$$E(\theta, \mathbf{t} \mid \mathcal{C}, \epsilon) = \sum_{i=1}^{M} \mathbb{I}(\|\mathbf{R}(\theta)\mathbf{p}_i + \mathbf{t} - \mathbf{q}_i\| \leq \epsilon) \tag{2}$$

where $\mathbb{I}$ is an indicator function that returns 1 if the input predicate is satisfied, and 0 otherwise, and ϵ is the inlier threshold. The value of parameter ϵ can be empirically determined through multiple experiments.

Therefore, our primary objective is to address the optimization problem

$$E^* = \max_{\theta, \mathbf{t}} E(\theta, \mathbf{t} \mid \mathcal{C}, \epsilon) \tag{3}$$

In essence, we are seeking the precise angle and translation vector, denoted as θ^* and $\mathbf{t}^*$, that results in the maximum objective value $E^* = E(\theta^*, \mathbf{t}^* \mid \mathcal{C}, \epsilon)$.

4. Algorithm Formulation

As depicted in Figure 1, after obtaining the correspondence set $\mathcal{C}$, our approach to solving Equation (3) primarily involves two steps. Initially, the FMP is applied to remove mismatches from set $\mathcal{C}$, thus transforming it into a significantly smaller subset $\mathcal{C}'$. Subsequently, we employ a deterministic 4-DOF Branch-and-Bound algorithm (4-DOF BnB) to search for the optimal θ^*, $\mathbf{t}^*$ within the subset $\mathcal{C}'$. To better illustrate the algorithmic processes, we begin by introducing the 4-DOF BnB algorithm, followed by a description of the FMP algorithm.

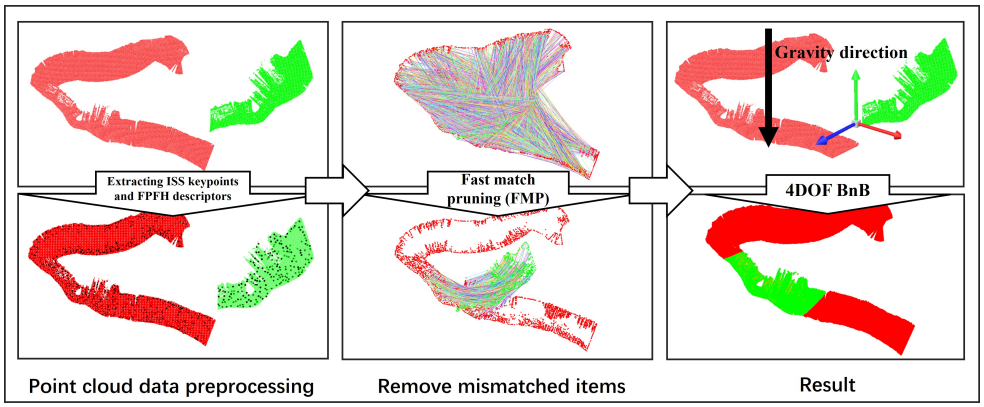


Figure 1. The overall algorithmic framework is as follows: Initially, point clouds are preprocessed, including downsampling, extracting Invariant Shape Signature (ISS) key points, and obtaining matching relations using the Fast Point Feature Histograms (FPFH) descriptor. Subsequently, the Fast Marching Pruning (FMP) algorithm is applied to eliminate mismatches within the correspondences. Finally, by aligning the gravity direction of the point cloud with the Z-axis direction, the three degrees of freedom for rotation are reduced to one, and the transformation matrix is computed using the BnB algorithm with four degrees of freedom.

4.1. Deterministic 4-BnB Algorithm for Registration

To derive the 4-BnB algorithm, we first rewrite (3) as

$$E^* = \max_{\mathbf{t}} U(\mathbf{t} \mid \mathcal{C}, \epsilon), \tag{4}$$

where

$$U(\mathbf{t} \mid \mathcal{C}, \epsilon) = \max_{\theta} E(\theta, \mathbf{t} \mid \mathcal{C}, \epsilon) \tag{5}$$

By reformulating Equation (3) as Equation (4), we can decompose the optimization task into two distinct steps: the deterministic rotation estimation and the translation search based on Branch and Bound (BnB). The following sections provide an in-depth discussion of these two steps.

4.1.1. Deterministic Rotation Estimation

The equation $U(\mathbf{t} \mid \mathcal{C}, \epsilon)$ is fully articulated as

$$U(\mathbf{t} \mid \mathcal{C}, \epsilon) = \max_{\theta} \sum_{i=1}^{M} \mathbb{I}(\|\mathbf{R}(\theta)\mathbf{p}_i - \tilde{\mathbf{q}}_i\| \leq \epsilon) \tag{6}$$

where $\tilde{\mathbf{q}}_i = \mathbf{q}_i - \mathbf{t}$. The evaluation of this function is tantamount to determining the rotation $\mathbf{R}(\theta)$ that maximizes the alignment of the set of point pairs $\{(\mathbf{p}_i, \tilde{\mathbf{q}}_i)\}_{i=1}^{M}$.

For each $\mathbf{p}_i$, applying the rotation $\mathbf{R}(\theta)$ over the entire range $\theta \in [0, 2\pi]$ generates a circular trajectory.

$$\text{circ}_i = \{\mathbf{R}(\theta)\mathbf{p}_i \mid \theta \in [0, 2\pi]\}. \tag{7}$$

It is inherently understood that circ_i reduces to a point in the circumstance where $\mathbf{p}_i$ is positioned on the z-axis. Define

$$\text{ball}_i(\epsilon) = \left\{\mathbf{q} \in \mathbb{R}^3 \mid \|\mathbf{q} - \tilde{\mathbf{q}}_i\| \leq \epsilon\right\} \tag{8}$$

and consider the ϵ-ball centered at $\tilde{\mathbf{q}}_i$. It is evident that the correspondence between the pair $(\mathbf{p}_i, \tilde{\mathbf{q}}_i)$ is achievable via $\mathbf{R}(\theta)$ if, and only if, there exists an intersection between circ_i and ball_i. Furthermore, the absence of an intersection between circ_i and ball_i incontrovertibly indicates that the ith pair exerts no influence on Equation (6).

For each i, denote

$$\text{int}_i = [\alpha_i, \beta_i] \subseteq [0, 2\pi] \tag{9}$$

and define the angular interval int_i such that $\mathbf{R}(\theta)\mathbf{p}_i$ is congruent to $\tilde{\mathbf{q}}_i$ within an ϵ threshold for every $\theta \in \text{int}_i$. The boundary values α_i, β_i are deducible through the analytic computation of circle-to-circle intersections. It is important to note that int_i is nullified if circ_i and ball_i are non-intersecting. For simplification in the subsequent discourse, we consider each int_i as a single contiguous interval. In practical applications, however, int_i can be segmented into two distinct intervals when its span exceeds the domain $[0, 2\pi]$. Consequently, the function $U(\mathbf{t} \mid \mathcal{C}, \epsilon)$ is amenable to being restated as

$$U(\mathbf{t} \mid \mathcal{C}, \epsilon) = \max_{\theta} \sum_{i=1}^{M} \mathbb{I}(\theta \in [\alpha_i, \beta_i]), \tag{10}$$

this scenario represents an instance of the max-stabbing problem.

4.1.2. BnB for Translation Search

Within the framework of addressing Equation (4), the BnB algorithm instigates the process by defining a hypercube $\mathbb{S}_0$ in the three-dimensional Euclidean space $\mathbb{R}^3$, encapsulating the optimal solution vector $\mathbf{t}^*$. The method proceeds to recursively segment $\mathbb{S}_0$ into octants. For every progeny subcube $\mathbb{S}$ within the parental hypercube $\mathbb{S}_0$, we assign $\mathbf{t}_\mathbb{S}$ as the centroid of $\mathbb{S}$. Subsequently, if $\mathbf{t}_\mathbb{S}$ yields a superior objective metric relative to the extant apex estimate $\hat{\mathbf{t}}$, the estimate is duly updated, $\hat{\mathbf{t}} \leftarrow \mathbf{t}_\mathbb{S}$. Conversely, if not, either

1. A determination may be reached to exclude $\mathbb{S}$ from further consideration;
2. Or the subcube $\mathbb{S}$ is subdivided into an octet of smaller hypercubes, whereupon the aforementioned procedural steps are iteratively applied.

In the asymptotic analysis, the estimator $\hat{\mathbf{t}}$ converges towards the optimal solution vector $\mathbf{t}^*$. Upon considering a subcube $\mathbb{S}$ in relation to the prevailing solution $\hat{\mathbf{t}}$, the exclusion of $\mathbb{S}$ is warranted if

$$\bar{U}(\mathbb{S} \mid \mathcal{C}, \epsilon) \leq U(\hat{\mathbf{t}} \mid \mathcal{C}, \epsilon), \tag{11}$$

where $\bar{U}(\mathbb{S} \mid \mathcal{C}, \epsilon)$ computes the superior limit of $U(\mathbf{t} \mid \mathcal{C}, \epsilon)$across the domain $\mathbb{S}$, that is to say,

$$\bar{U}(\mathbb{S} \mid \mathcal{C}, \epsilon) \geq \max_{\mathbf{t} \in \mathbb{S}} U(\mathbf{t} \mid \mathcal{C}, \epsilon). \tag{12}$$

The underlying principle posits that, should condition (11) be satisfied, the existence of a solution superior to $\hat{\mathbf{t}}$ within $\mathbb{S}$ is an impossibility. In the context of our research, the upper bound is derived as

$$\bar{U}(\mathbb{S} \mid \mathcal{C}, \epsilon) = U(\mathbf{t}_\mathbb{S} \mid \mathcal{C}, \epsilon + d_\mathbb{S}), \tag{13}$$

wherein $d_\mathbb{S}$ denotes one-half of the diagonal extent of the subcube $\mathbb{S}$. It is pertinent to acknowledge that the computation of this bound is tantamount to assessing the function U, a process that can be expedited through the application of max-stabbing.

4.2. Fast Match Pruning Algorithm

Rather than directly applying the BnB algorithm to the match set $\mathcal{C}$, our methodology commences with a preprocessing phase to curtail $\mathcal{C}$ to a markedly condensed subset $\mathcal{C}'$, subsequent to which BnB is performed on $\mathcal{C}'$. It is of significant note that this diminution process can be conducted in such a manner that $\mathcal{C}'$ retains the optimal solution, i.e.,

$$\theta^*, \mathbf{t}^* = \arg\max_{\theta, \mathbf{t}} E(\theta, \mathbf{t} \mid \mathcal{C}, \epsilon) = \arg\max_{\theta, \mathbf{t}} E(\theta, \mathbf{t} \mid \mathcal{C}', \epsilon). \tag{14}$$

Consequently, the execution of the BnB algorithm is considerably expedited, yet it keeps the ability to ascertain the optimum with respect to the initial, comprehensive match set.

Define $\mathcal{I}^*$ as the subset of $\mathcal{C}$ that is congruently aligned by the rotation θ^* and translation $\mathbf{t}^*$, formally,

$$\|\mathbf{R}(\theta^*)\mathbf{p}_i + \mathbf{t}^* - \mathbf{q}_i\| \leq \epsilon \quad \forall(\mathbf{p}_i, \mathbf{q}_i) \in \mathcal{I}^*. \tag{15}$$

If the following condition holds

$$\mathcal{I}^* \subseteq \mathcal{C}' \subseteq \mathcal{C}, \tag{16}$$

it consequently ensues that inequality (16) is upheld. Therefore, the preprocessing stratagem entails the exclusive elimination of correspondences residing in $\mathcal{C} \backslash \mathcal{I}^*$. Due to the article's length restrictions, the steps for algorithmic resolution are provided in Algorithm 1. A more detailed implementation method can be found in the work [31].

Algorithm 1 Fast match pruning (FMP)

Require: Initial matches $\mathcal{C}$, the inlier threshold ϵ.
1: $\underline{E} \leftarrow 0, \mathcal{C}' \leftarrow \mathcal{C}$.
2: **for** $k = 1, \ldots, M$ **do**
3: Compute $\bar{E}_k$.
4: **if** $\bar{E}_k < \underline{E}$ **then**
5: $\mathcal{C}' \leftarrow \mathcal{C}$.
6: **else**
7: Re-evaluate $\underline{E}$ using the corresponding solution of $\bar{E}_k$.
8: **end if**
9: **end for**
10: Remove from $\mathcal{C}'$ the remaining (p_k, q_k) whose $\bar{E}_k < \underline{E}$.
11: **return** $\mathcal{C}'$.

5. Experiments

The experiments were divided into two parts: testing on a dataset and testing in a real-world scenario. All experiments were carried out on a computer with an Intel Core i5-10400F CPU and 8 GB of RAM.

We conducted comparisons against the state-of-the-art classical methods in the field of point cloud registration. The evaluation metrics included rotation error, translation error, and runtime. The methods compared are listed as follows:

- RANSAC [14]: an method that utilizes a random sampling approach to find correspondences and estimate geometric transformations between two data sets with the use of pairs of points.
- LM [32]: the 4-DOF LM simplifies optimization for planar movement with four degrees of freedom.
- GTA [33]: a stochastic outlier removal method.
- K4PCS [34]: key-point-based 4PCS speeds up point cloud alignment by focusing on key features.

In the testing methodology, the RANSAC method was tested with two different maximum iteration counts. The first was set to 50,000 iterations, referred to as RANSAC-min-iter. The second was set to $corr * (corr - 1)/2$ iterations, termed RANSAC-max-iter, where $corr$ denotes the number of correspondences. For the LM, GTA, and K4PCS algorithms, default parameters were used. The performance and accuracy of each method were evaluated using the rotation error, denoted as e_{rot}, and translation error, denoted as e_{trans}. These errors are defined as follows:

$$e_{rot} = arccos(\frac{Tr(\mathbf{R}_{gt}^{-1}\mathbf{R}^*) - 1}{2}) \tag{17}$$

$$e_{trans} = \|\mathbf{t}_{gt} - \mathbf{t}^*\| \tag{18}$$

where $\mathbf{t}_{gt}$ and $\mathbf{R}_{gt}$ represent the ground-truth translation and rotation, respectively, while $\mathbf{t}^*$ and $\mathbf{R}^*$ denote the estimated solution for translation and rotation. The function $Tr()$ denotes the trace of a matrix.

5.1. Public Dataset Experiment

The dataset used for testing, DotsonEast, originates from the work of [35]. It is a semi-synthetic MBES (Multi-Beam Echo Sounder) registration dataset, constructed from autonomous underwater vehicle (AUV) missions in the western Antarctic region. The authors of that work configured each sub-map to consist of 100 consecutive pings, with a step size of 20 pings. Consequently, two consecutive sub-maps had an 80% data overlap. Using this method, sub-maps with overlap percentages of 20%, 40%, 60%, 80%, and 100% can be derived. Based on varying overlap ratios, each set of test data contained 941, 942, 943, 944, and 945 pairs of registration data, respectively.

In the experiments, pairs of sub-maps for registration were synthesized by applying rotations, translations, and adding noise to each sub-map. For rotations, we sampled within the range of [0, 10°] for the Z-axis, while keeping the rotations around the XY axes constant. For translations, we sampled within the range of [−40, 40] meters for the X and Y axes, and within the range of [−2, 2] meters for the Z-axis. The test set was categorized into three types based on the type of noise added: clean, crop, and jitter.

For each pair of tested point clouds, we applied voxel downsampling with a resolution of 1 m to achieve uniform point density. Subsequently, we extracted ISS key points and computed FPFH for key-point matching, resulting in the correspondence set $\mathcal{C}$.

Based on Figure 2, this study presents a detailed comparison of method performance across various noise conditions. Specifically, the chart sequentially shows experimental results for clean, crop, and jitter conditions from top to bottom. The chart clearly demonstrates that the proposed FMP + BnB method maintained relatively stable and accurate performance across all levels of overlap. Notably, under low-overlap conditions, the FMP + BnB method exhibited a rotational error ranging from 0.11 to 0.25 and a translation error ranging from 52 to 110, indicating a distinct performance advantage compared to other methods. As the overlap rate increased, a general trend of decreasing error was observed for all methods, as higher overlap rates provided more redundant information, which aided in improving registration accuracy. At 100% overlap, methods such as RANSAC-max-iter, LM, GTA, and K4PCS achieved performance comparable to that of FMP + BnB, whereas RANSAC-min-iter consistently showed larger errors. These results underscore the importance of the number of iterations for the RANSAC method in practical applications.

Building upon the experimental results, we further explored the potential reasons for higher errors under certain conditions or with specific methods. For instance, the RANSAC-min-iter method performed poorly under low-overlap conditions potentially because it relied on a maximum number of iterations to converge to a solution, which may not have been sufficient to find an optimal solution in the absence of adequate information. Additionally, the GTA method could exhibit increased errors in certain scenarios due to its sensitivity to noise. While the FMP + BnB method performed stably in most cases, it too faced challenges under extreme noise conditions, such as crop noise, indicating the need for further algorithm optimization in future work to enhance its robustness in complex environments.

In terms of computational time, as illustrated in Figure 3a, the runtime refers to the average of three runs under three different noise conditions: clean, crop, and jitter. It is evident that the RANSAC-max-iter approach required the longest execution time due to its numerous iterations, ranging from 4048 to 5692 s. The K4PCS approach had the second-longest runtime, approximately 2300 s. In contrast, the RANSAC-min-iter, LM, and GTA approaches required less time, ranging from 300 to 400 s. The FMP + BnB approach had an execution time ranging from 463 to 881 s, with an average of 0.48 to 0.92 s for each registration operation. Additionally, comparative experiments were conducted on a computer equipped with an Intel Core i5-13500H CPU and 16 GB of RAM, as illustrated in Figure 3b. It can be observed that with improvements in CPU and memory performance, the runtime of different methods decreased to some extent. However, the relative runtime among the methods remained unchanged overall. Given the unique characteristics of the sensors and the operational environment, underwater point cloud registration cannot be performed in real time and necessitates offline processing after data collection. Therefore, the FMP + BnB approach offers an acceptable running time while providing a satisfactory solution.

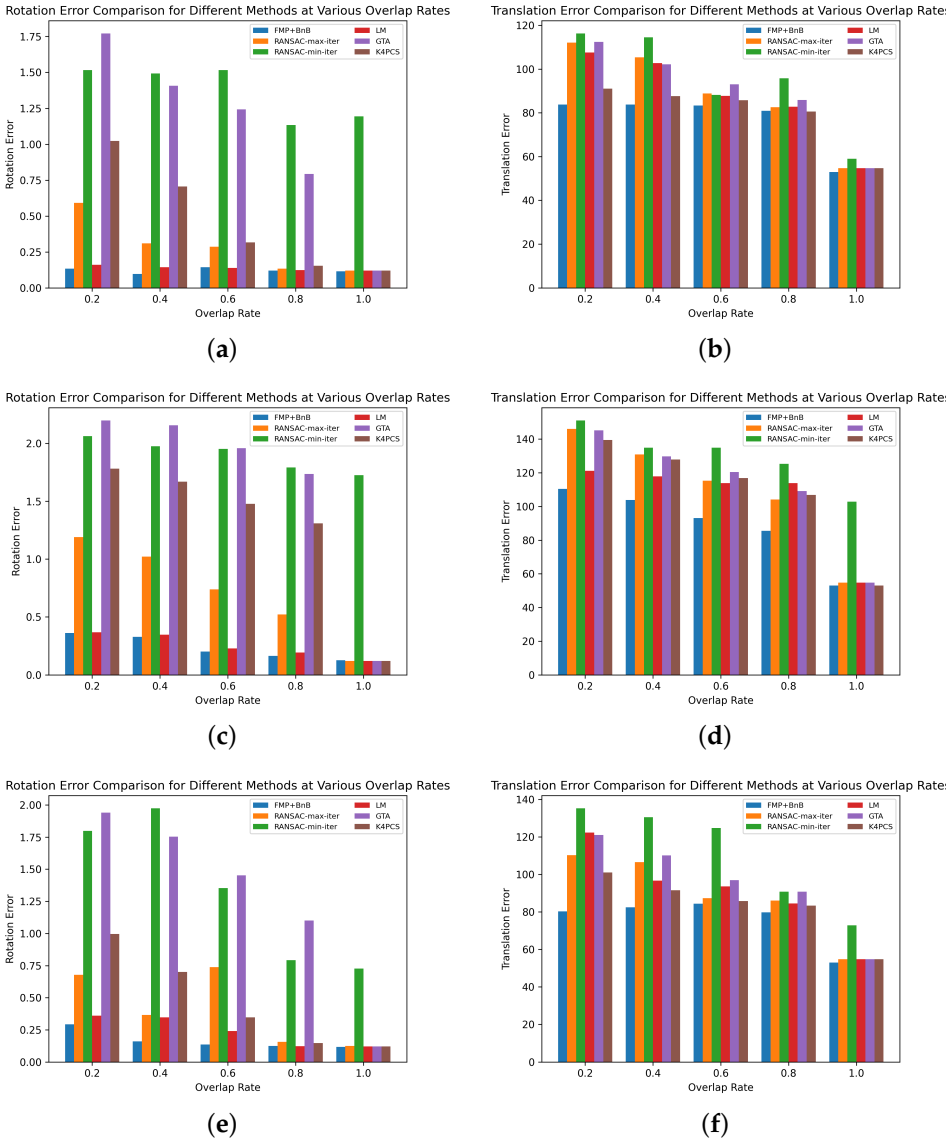


Figure 2. Subfigures (**a**,**c**,**e**) represent rotational errors, while subfigures (**b**,**d**,**f**) denote translational errors. From top to bottom, they correspond to errors under three types of noise conditions: clean, crop, and jitter.

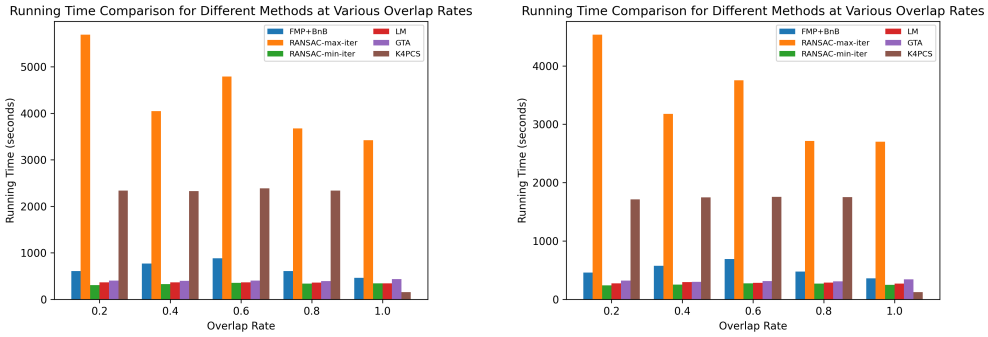


Figure 3. Runtime comparison of different methods across different hardware devices. Figure (**a**) is run on a device equipped with an Intel Core i5-10400F CPU and 8 GB of RAM, while Figure (**b**) is run on a device with an Intel Core i5-13500H CPU and 16 GB of RAM.

5.2. Real-World Lake Dataset Experiments

First, we introduce the experimental site, platform, and data. Following this, we describe the preprocessing phase of the experimental data, which supplements aspects not covered in the dataset experiments. Finally, registration experiments are performed on real-world data.

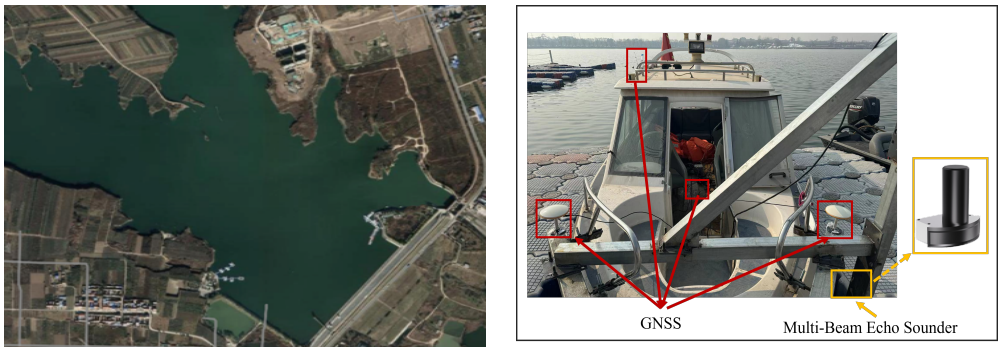
5.2.1. Platform Setup and Data Preparation

The experiments utilized an HDY-BD400D MBES; the primary performance parameters of which are detailed in Table 1. The construction of the experimental site and platform is shown in Figure 4.

Table 1. HDY-BD400D primary performance specifications.

Parameters	Metrics
Operating frequency	400 kHz–700 kHz, real-time continuously adjustable with a step size of 1 kHz
Cross-track beam width	1°@400 kHz; 0.5°@700 kHz
Along-track beam width	1°@400 kHz; 0.5°@700 kHz
Number of beams	256/512 (Equal angle/equal distance)
Sector opening angle	10°–180° real-time continuously adjustable
Range	200 m @ 400 KHz
Pulse width	10 µs–800 µs
Ping rate	Up to 50 Hz

Data were collected and processed with reference to work [4], yielding the experimental data. We extracted three pairs of point clouds with varying overlap rates to serve as experimental data, denoted as p1, p2, and p3. For each pair, the source point cloud was represented by **P**, and the target point cloud by **Q**. Each target point cloud **Q** underwent random translations ranging from 0 to 5 m along the x, y, and z axes, and rotations around the z-axis ranging from 0 to 60 degrees. The Z-axis of each point set is aligned with the gravitational direction of the IMU. The three pairs of point clouds are depicted in Figure 5.



(**a**) (**b**)

Figure 4. Figure (**a**) presents the experimental site, a lake encompassing an area of over 10,000 hectares with a maximum depth of 20 m, characterized by a diverse underwater topography. Figure (**b**) displays the constructed experimental platform, which primarily comprises a multibeam sonar and a suite of inertial navigation systems. The inertial navigation system was utilized to furnish IMU and GPS data, facilitating the construction of the point cloud.

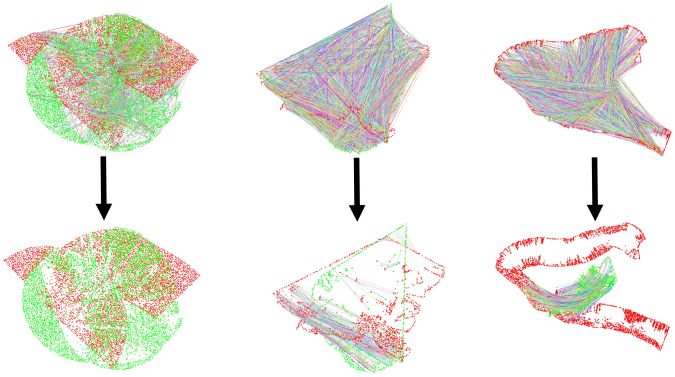


Figure 5. The corresponding relationships within set $\mathcal{C}$ were contrasted before and after the application of FMP to eliminate mismatches. To better showcase these correspondences, the centroids of two point clouds were moved to the origin, and sparse feature points were utilized.

5.2.2. Data Preprocessing

The correspondence set was obtained using the same method as described in Section 5.1. For each pair of point clouds, the original number of points and the number of extracted feature points are shown in Table 2.

Table 2. The original number of points and the number of key points for each pair of point clouds.

Data	P	Q	P_{key}	Q_{key}
p1	36,956	46,648	5048	5820
p2	54,912	31,170	1344	734
p3	86,776	16,962	3744	1209

Upon the generation of the set, the FMP method was utilized to remove mismatches, resulting in a refined match set. As evident from Table 3, there was a notable reduction in the number of elements within the set, hence providing high-quality correspondences for the subsequent registration process. The quantity of correspondences before and after processing, along with the runtime of the method, are depicted in Table 3. The correspondences are visually displayed in Figure 5.

Table 3. Results of the FMP method execution.

Data	p1	p2	p3
Before FMP	1321	5148	8920
After FMP	18	208	674
Proportion(%)	1.36	4.04	7.56
Running time (ms)	77	271	1072

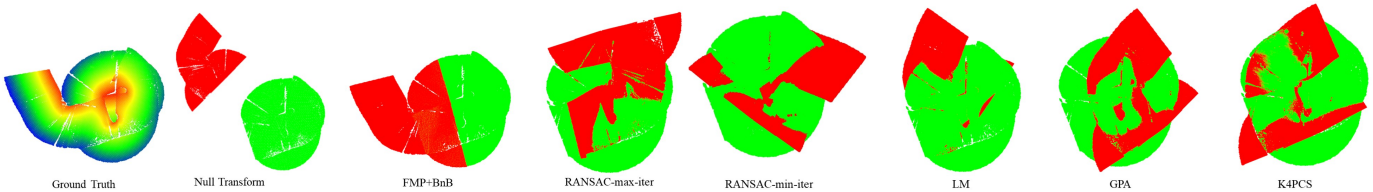
5.2.3. Registration Test

If the rotation error exceeded 0.5 degrees or the translation error exceeded 1 m, the registration was deemed to have failed. According to Table 4, the method proposed in this paper successfully registered all datasets. In contrast, the RANSAC-max-iter method failed once, the RANSAC-min-iter method failed twice, the LM method failed twice, the GTA method failed once, and the K4PCS method failed twice. These outcomes can be attributed to the low overlap rate between point clouds P and Q in the P1 dataset, coupled with a large number of points, which led to the failure of all methods except for the one proposed in this paper. Conversely, in the P3 dataset, there was significant overlap between the target point cloud Q and the source point cloud P, and P3 was rich in local features, allowing all methods to successfully perform registration.

Table 4. The rotational error (°), translational error (m), and running time (ms) for each method on every pair of point clouds.

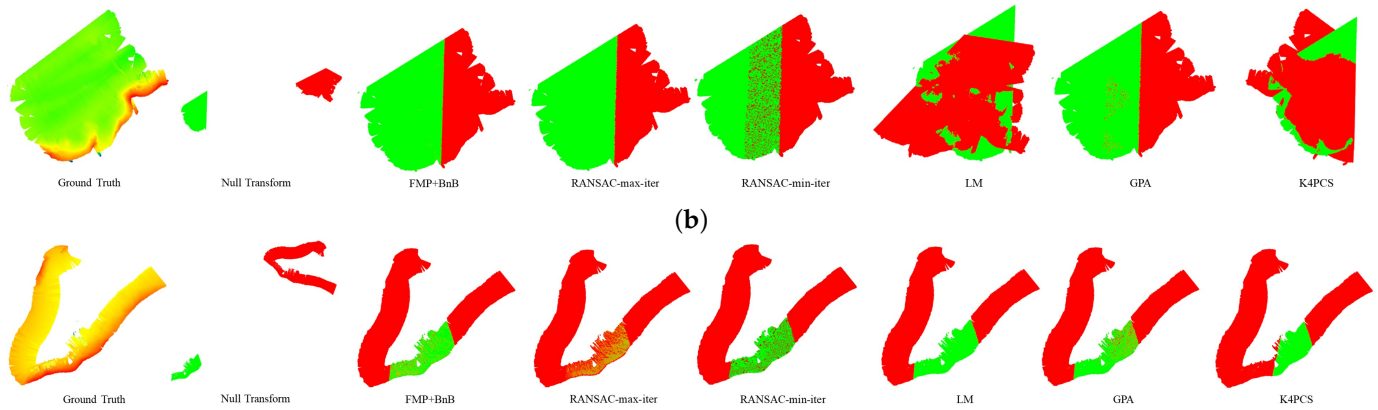
Evaluation Metrics	Data	FMP + BnB	RANSAC-Max-Iter	RANSAC-Min-Iter	LM	GTA	K4PCS
Rotation error	p1	0.047	89.998	2.650	49.561	70.543	136.39
	p2	0.055	0.048	0.054	40.33	0.058	178
	p3	0.012	0.058	0.037	0.031	0.058	0.024
Translation error	p1	0.726	1429.414	1848.339	814.469	1084.906	1858.82
	p2	0.274	0.024	3.630	750.481	0.079	1416.354
	p3	0.334	0.458	0.014	0.001	0.012	0.010
Running time (device 1)	p1	2953	26,143	5109	2177	2165	159,253
	p2	1408	687	2434	603	1008	7913
	p3	3628	1345	2617	1297	2579	115,093
Running time (device 2)	p1	2213	19,557	3918	1660	1619	122,673
	p2	1050	521	1939	452	748	6259
	p3	2811	1021	1950	968	2036	88,598

In terms of registration accuracy, as shown in Table 4, the FMP + BnB method exhibited the most stable performance, whereas the RANSAC method showed higher uncertainty. With an increase in the number of point clouds, the runtime of the RANSAC method increased rapidly. In contrast, the FMP + BnB method, the LM method, and the GTA method maintained relatively stable runtimes. Figure 6 illustrates the registration results for three pairs of data.



(**a**)

Figure 6. *Cont.*



(**b**)

(**c**)

Figure 6. Subfigures (**a**–**c**) represent the registration results of each method on the p1, p2, and p3 matching pairs respectively. In these images, red indicates the source point set, while green represents the target point set.

6. Conclusions

In this paper, we presented a fast and deterministic point cloud registration method based on MBES technology for underwater environments. To address the pervasive noise and outliers in underwater point clouds, we employed a deterministic optimization technique called BnB to ensure a globally optimal solution. Furthermore, by aligning the Z-axis of the point cloud with the gravitational direction of the IMU, we reduced the rotational degrees of freedom from three to a single yaw rotation, thus decreasing the dimensionality of the solution space. Given that key-point matching often results in numerous erroneous matches, we introduced a strategy for excluding these false matches, significantly enhancing the efficiency of our approach. Experiments conducted on both public and real-world lake datasets validated the effectiveness of the proposed method in underwater point cloud registration. Future work will focus on enhancing the computational speed of the algorithm and refining the process of key-point extraction and matching. This includes the exploration of more advanced key-point detection algorithms that demonstrate robustness to noise, along with the development of sophisticated matching strategies capable of addressing a broader range of underwater scenarios. These scenarios will be characterized by high noise levels and point clouds with varying densities. Deep learning techniques will be integrated to improve the robustness and adaptability of the algorithm.

Author Contributions: L.Z. was responsible for manuscript writing, method implementation, data analysis, and data processing. L.C. and F.Z. were responsible for method design, guidance on paper writing, and revisions. T.T. and C.C. were responsible for data collection and processing. All authors have read and agreed to the published version of the manuscript.

Funding: This research was funded by the National Natural Science Foundation of China (52171322 and 62073232) and the Fundamental Research Funds for the Central Universities (G2024KY0602).

Institutional Review Board Statement: Not applicable.

Informed Consent Statement: Not applicable.

Data Availability Statement: The data can be accessed at https://github.com/ZLIANG-code/MBES-datasets (accessed on 25 December 2024).

Acknowledgments: We would like to acknowledge the facilities and technical assistance provided by the Key Laboratory of Unmanned Underwater Transport Technology.

Conflicts of Interest: The authors declare no conflicts of interest.

Abbreviations

The following abbreviations are used in this manuscript:

MBES	Multibeam Echo Sounder
BnB	Branch and Bound
IMU	Inertial Measurement Unit
RANSAC	Random Sample Consensus
ICP	Iterative Closest Point
FMP	Fast Marching Pruning
DOF	Degree of freedom
iEKF	Iterative Extended Kalman Filter
GICP	Generalized Iterative Closest Point

References

1. Joshi, B.; Xanthidis, M.; Roznere, M.; Burgdorfer, N.J.; Mordohai, P.; Li, A.Q.; Rekleitis, I. Underwater exploration and mapping. In Proceedings of the IEEE OES AUV Symposium, Singapore, 19–21 September 2022; pp. 1–7.
2. Hollinger, G.A.; Englot, B.; Hover, F.S.; Mitra, U.; Sukhatme, G.S. Active planning for underwater inspection and the benefit of adaptivity. *Int. J. Robot. Res.* **2013**, *32*, 3–18. [CrossRef]
3. Brown, C.J.; Blondel, P. Developments in the application of multibeam sonar backscatter for seafloor habitat mapping. *Appl. Acoust.* **2009**, *70*, 1242–1247; [CrossRef]
4. Zhang, F.; Tan, T.; Hou, X.; Zhao, L.; Cao, C.; Wang, Z. Underwater mapping and optimization based on multibeam echo sounders. *J. Mar. Sci. Eng.* **2024**, *12*, 1222. [CrossRef]
5. Huang, X.; Mei, G.; Zhang, J.; Abbas, R. A comprehensive survey on point cloud registration. *arXiv* **2021**, arXiv:2103.02690.
6. Besl, P.J.; McKay, N.D. A method for registration of 3-d shapes. *IEEE Trans. Pattern Anal. Mach. Intell.* **1992**, *14*, 239–256. [CrossRef]
7. Yan, L.; Wei, P.; Xie, H.; Dai, J.; Wu, H.; Huang, M. A new outlier removal strategy based on reliability of correspondence graph for fast point cloud registration. *IEEE Trans. Pattern Anal. Mach. Intell.* **2023**, *45*, 7986–8002. [CrossRef] [PubMed]
8. Li, J.; Shi, P.; Hu, Q.; Zhang, Y. Qgore: Quadratic-time guaranteed outlier removal for point cloud registration. *IEEE Trans. Pattern Anal. Mach. Intell.* **2023**, *45*, 11136–11151. [CrossRef] [PubMed]
9. Bustos, Á.P.; Chin, T. Guaranteed outlier removal for point cloud registration with correspondences. *IEEE Trans. Pattern Anal. Mach. Intell.* **2018**, *40*, 2868–2882. [CrossRef] [PubMed]
10. Fischler, M.A.; Bolles, R.C. Random sample consensus. In *Communications of the ACM*; ACM: New York, NY, USA, 1981; pp. 381–395.
11. Salti, S.; Tombari, F.; Stefano, L.D. A performance evaluation of 3d keypoint detectors. In Proceedings of the 2011 International Conference on 3D Imaging, Modeling, Processing, Visualization and Transmission, Hangzhou, China, 16–19 May 2011; Volume 102, pp. 236–243.
12. Li, H. Consensus set maximization with guaranteed global optimality for robust geometry estimation. In Proceedings of the 2009 IEEE 12th International Conference on Computer Vision, Kyoto, Japan, 29 September–2 October 2009; pp. 1074–1080.
13. Le, H.; Chin, T.; Eriksson, A.; Do, T.; Suter, D. Deterministic approximate methods for maximum consensus robust fitting. *IEEE Trans. Pattern Anal. Mach. Intell.* **2021**, *43*, 842–857. [CrossRef] [PubMed]
14. Fischler, M.A.; Bolles, R.C. Random sample consensus: A paradigm for model fitting with applications to image analysis and automated cartography. *Commun. ACM* **1981**, *24*, 381–395. [CrossRef]
15. Horst, R.; Tuy, H. *Global Optimization: Deterministic Approaches*; Springer: Berlin/Heidelberg, Germany, 1992.
16. Li, X.; Liu, Y.; Xia, Y.; Lakshminarasimhan, V.; Cao, H.; Zhang, F.; Stilla, U.; Knoll, A. Fast and deterministic (3+1)dof point set registration with gravity prior. *ISPRS J. Photogramm. Remote Sens.* **2023**, *199*, 118–132. [CrossRef]
17. Rusinkiewicz, S.; Levoy, M. Efficient variants of the icp algorithm. In Proceedings of the Third International Conference on 3-D Digital Imaging and Modeling, Quebec City, QC, Canada, 28 May–1 June 2001.
18. Li, J.; Hu, Q.; Zhang, Y.; Ai, M. Robust symmetric iterative closest point. *ISPRS J. Photogramm. Remote Sens.* **2022**, *185*, 219–231. [CrossRef]
19. Zhang, X.; Yang, J.; Zhang, S.; Zhang, Y. 3d registration with maximal cliques. *arXiv* **2023**, arXiv:2305.10854.
20. Zhong, Y. Intrinsic shape signatures: A shape descriptor for 3d object recognition. In Proceedings of the 2009 IEEE 12th International Conference on Computer Vision Workshops, ICCV Workshops, Kyoto, Japan, 27 September–4 October 2009.
21. Abdelhafiz, D.; Youssef, B.; Sheta, W.; Hassan, H. Interest point detection in 3d point cloud data using 3d sobel-harris operator. *Int. J. Pattern Recognit. Artif.* **2015**, *29*, 150710022059009.

22. Steder, B.; Rusu, B.; Konolige, K.; Burgard, W. Narf: 3D Range Image Features for Object Recognition. 2010. Available online: https://citeseerx.ist.psu.edu/document?repid=rep1&type=pdf&doi=e0701662a370622a1cdbb7c6a83bbede3d0e6c23 (accessed on 25 December 2024).
23. Li, Q.; Huang, X.; Shuanggao, L.; Deng, Z. Feature extraction from point clouds for rigid aircraft part inspection using an improved harris algorithm. *Meas. Sci. Technol.* **2018**, *29*, 115202. [CrossRef]
24. Rusu, R.B.; Blodow, N.; Beetz, M. Fast point feature histograms (fpfh) for 3d registration. In Proceedings of the 2009 IEEE International Conference on Robotics and Automation, Kobe, Japan, 12–17 May 2009.
25. Shi, J.; Yang, H.; Carlone, L. Robin: A graph-theoretic approach to reject outliers in robust estimation using invariants. In Proceedings of the 2021 IEEE International Conference on Robotics and Automation (ICRA), Xi'an, China, 30 May–5 June 2021; pp. 13820–13827.
26. Raguram, R.; Frahm, J.; Pollefeys, M. Exploiting uncertainty in random sample consensus. In Proceedings of the 2009 IEEE 12th International Conference on Computer Vision, Kyoto, Japan, 29 September–2 October 2009; pp. 2074–2081.
27. Raguram, R.; Chum, O.; Pollefeys, M.; Matas, J.; Frahm, J. Usac: A universal framework for random sample consensus. *IEEE Trans. Pattern Anal. Mach. Intell.* **2013**, *35*, 2022–2038. [CrossRef] [PubMed]
28. Rahman, M.; Li, X.; Yin, X. Dl-ransac: An improved ransac with modified sampling strategy based on the likelihood. In Proceedings of the 2019 IEEE 4th International Conference on Image, Vision and Computing (ICIVC), Xiamen, China, 5–7 July 2019; pp. 463–468.
29. Choy, C.; Park, J.; Koltun, V. Fully convolutional geometric features. In Proceedings of the 2019 IEEE/CVF International Conference on Computer Vision (ICCV), Seoul, Republic of Korea, 27 October–2 November 2019.
30. Huang, S.; Gojcic, Z.; Usvyatsov, M.; Wieser, A. Konrad Schindler Predator: Registration of 3d point clouds with low overlap. In Proceedings of the 2021 IEEE/CVF Conference on Computer Vision and Pattern Recognition (CVPR), Nashville, TN, USA, 20–25 June 2021.
31. Cai, Z.; Chin, T.; Bustos, A.P.; Schindler, K. Practical optimal registration of terrestrial lidar scan pairs. *ISPRS J. Photogramm. Remote Sens.* **2019**, *147*, 118–131. [CrossRef]
32. Qi, Z.; Park, J.; Koltun, V. Fast Global Registration. In Proceedings of the 14th European Conference, Amsterdam, The Netherlands, 11–14 October 2016; pp. 766–782.
33. Albarelli, A.; Rodola, E.; Torsello, A. A game-theoretic approach to fine surface registration without initial motion estimation. In Proceedings of the 2010 IEEE Computer Society Conference on Computer Vision and Pattern Recognition, San Francisco, CA, USA, 13–18 June 2010.
34. Theiler, P.; Wegner, J.; Schindler, K. Keypoint-based 4-points congruent sets–automated marker-less registration of laser scans. *ISPRS J. Photogramm. Remote Sens.* **2014**, *96*, 149–163. [CrossRef]
35. Ling, L.; Zhang, J.; Bore, N.; Folkesson, J.; Wåhlin, A.K. Benchmarking classical and learning-based multibeam point cloud registration. In Proceedings of the 2024 IEEE International Conference on Robotics and Automation (ICRA), Yokohama, Japan, 13–17 May 2024; pp. 6118–6125.

Disclaimer/Publisher's Note: The statements, opinions and data contained in all publications are solely those of the individual author(s) and contributor(s) and not of MDPI and/or the editor(s). MDPI and/or the editor(s) disclaim responsibility for any injury to people or property resulting from any ideas, methods, instructions or products referred to in the content.